small
NANO MICRO
www.small-journal.com

Osmotic Effects in Track-Etched Nanopores

Pavel Y. Apel, Irina V. Blonskaya, Nikolay E. Lizunov, Katarzyna Olejniczak, Oleg L. Orelovitch, María E. Toimil-Molares, and Christina Trautmann*

Asymmetrically etched ion-track membranes attract great interest for both fundamental and technical reasons because of a large variety of applications. So far, conductometric measurements during track etching provide only limited information about the complicated asymmetric etching process. In this paper, monitoring of osmotic phenomena is used to elucidate the initial phase of nanopore formation. It is shown that strong alkaline solutions generate a considerable osmotic flow of water through newborn conical pores. The interplay between diffusion and convection in the pore channel results in a substantially nonlinear alkali concentration gradient and a rapid change in the pore geometry after breakthrough. Similar phenomena are observed in experiments with cylindrical track-etched pores of 15–30 nm in radius. A theoretical description of the diffusion–convection processes in the pores is provided.

1. Introduction

Osmosis is usually defined as a phenomenon of net water movement across a semipermeable membrane driven by an osmotic pressure difference. Relatively small attention has been paid to osmotic effects in permeable, i.e., leaky pores. However, in biology it is well-established that biological membranes are not perfectly semipermeable barriers, and that the description of osmotic transport has to consider both solvent and solute fluxes through the pores.[1–8] A bimodal mechanism of solvent flow through a biological pore has been suggested. Depending on the pore radius/solute size ratio, either diffusive or viscous flow of the solvent dominates.[4,5] To date, merely pores with a radius smaller than 1 nm have been considered, thus reflecting the special importance of osmotic effects in biological matter. For the case of larger pore radii, on the order of 10 nm, only solutions with high-molecular weight solutes have been studied.[9,10] This situation has resulted from the long-standing concept that, for osmotic phenomena, "the osmotic pressures of lipid-insoluble solutes are effective across cell membranes, whereas only osmotic pressures of macromolecular solutes are effective across capillary membranes."[7]

The technique of ion-track etching provides unique opportunities for developing microporous and nanoporous membranes, the transport properties of which can be finely tuned by tailoring the size, geometry, and number of pores.[11,12] The pore radius can be as small as several nanometers. In recent years, special interest has been devoted to so-called conical track-etched nanopores. Their fabrication involves the irradiation of a polymer foil with accelerated ions followed by asymmetric chemical etching. Typically, the foil is etched from one side with a strong etchant solution while the other side of the foil faces a relatively dilute stopping solution.[13,14] The chemical stopping by neutralization of the etchant at the moment of pore breakthrough is additionally supported by electrical stopping. A positive potential is applied to an electrode inserted into the etchant solution so that the OH^- ions or OCl^- ions (for polyethylene terephthalate and polyimide foils, respectively) are pulled out from the newborn pore which stops its further growth.[14] The resulting pore has an approximately conical shape with a large opening of the order of hundreds of nanometers and a small opening, called the pore tip, of only several nanometers in diameter. Asymmetric pores exhibit ionic current rectification in electrolyte solutions, an effect comprising the basis of many potential applications.[15–22] The process of pore formation and the properties of the pores have remained a subject of considerable interest and extensive studies.[23–35] However, no attention has been paid to the fact that the asymmetric etching is characterized by a very high salinity gradient across the foil that should inevitably lead to an intense osmotic flow of water from the stopping solution to the etchant solution. Only very recently, the essential role of osmotic phenomena under

Prof. P. Y. Apel, I. V. Blonskaya, N. E. Lizunov, K. Olejniczak, O. L. Orelovitch
Flerov Laboratory of Nuclear Reactions
Joint Institute for Nuclear Research
Joliot-Curie str. 6, 141980 Dubna, Russia
E-mail: apel@jinr.ru
Prof. P. Y. Apel
Department of Chemistry, New Technologies and Materials
Dubna State University
Universitetskaya str. 19, 141980 Dubna, Russia
K. Olejniczak
Department of Chemistry
Nicolaus Copernicus University
Gagarina str. 7, 87–100 Torun, Poland
Dr. M. E. Toimil-Molares, Prof. C. Trautmann
GSI Helmholtzzentrum für Schwerionenforschung GmbH
64291 Darmstadt, Germany
Prof. C. Trautmann
Materialwissenschaft
Technische Universität Darmstadt
Alarich-Weiss-Straße 2, 64287 Darmstadt, Germany
The ORCID identification number(s) for the author(s) of this article can be found under https://doi.org/10.1002/smll.201703327.

DOI: 10.1002/smll.201703327

asymmetric etching conditions has been confirmed experimentally.[36] The influence of osmotic flow on the pore evolution was elucidated from field-emission scanning electron microscopy (FESEM) images, taken at different stages of etching after pore breakthrough, i.e., when the etchant solution mixes with the stopping solution. The convective flow generated by the osmotic pressure was directly determined by measuring the increase in etchant solution volume in a cell with a multitrack sample inside. The osmotic flux was demonstrated to depend on the acidity of the stopping solution. A tentative explanation was suggested to account for the observed effect.

The aim of this work is to gain a deeper insight into the mechanisms of osmotic phenomena taking place in ion track etching. The influence of the stopping solution on the asymmetric etching process is analyzed. We also show that pores with radii of several tens of nanometers can exhibit osmotic flow in solutions of inorganic species, i.e., molecules and ions two orders of magnitude smaller than the pore radii. Finally, we demonstrate that, using osmotic effects, the shape of track-etched pores can be modified in a controlled way. The resulting pore shape is determined by the balance between the diffusive and convective transport of the etchant molecules inside the pore.

2. Results and Discussion

2.1. Single-Track Asymmetric Etching

The asymmetric etching of single tracks with the simultaneous application of a bias voltage is a necessary stage in the preparation of a nanopore-based nanofluidic diode. **Figure 1**A shows a typical electric current versus etching time diagram recorded for a single ion track in a polyethylene terephthalate (PET) foil. At the moment of breakthrough, t_b, the formation of a contiguous pore is signaled by a sudden rise in the current of up to 0.05-0.5 nA. After breakthrough, the electrical current does not monotonically grow but fluctuates around a slowly increasing mean value and the pore tip does not change much in size. At the moment of breakthrough, the etchant is diluted with stopping solution in the tip region. In the presence of an acid, partial neutralization occurs. In addition, the activity of the etchant in the tip region is assumed to decrease because of the electric field ("stopping voltage") that pulls hydroxide ions out from the tip opening. The relative contributions of these factors remain to be established. Figure 1B shows the results of the current measurements when the bias voltage was periodically switched on and off for 5 min. Every time the electric field was switched on, the current reached a higher value than at the end of the last cycle. Within the 5 min time interval that the bias voltage is applied to the membrane, the current goes down. An obvious reason for that is the replacement of highly mobile hydroxide ions with less mobile chlorine anions in the pore. Though the average value of the ion current tends to generally increase within a 1 h time interval after breakthrough, not each on–off cycle has a higher amplitude than the previous cycle. Therefore, even in the absence of an electric field the pore grows slowly and nonmonotonically.

The electric measurements obviously allow monitoring of the initial stage of the pore etching, but the process of the measurement itself impacts the object under study. It is known that, at

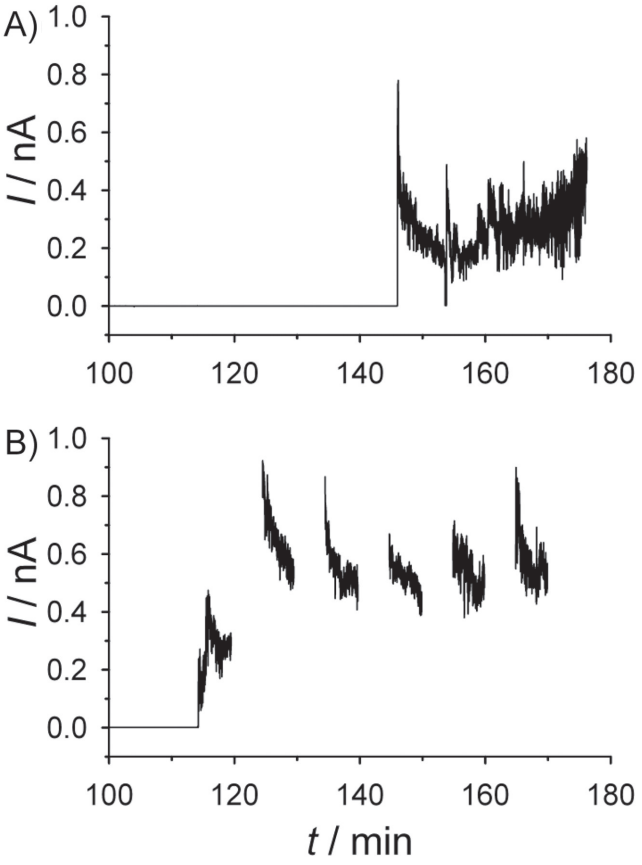

Figure 1. Electric current (I) versus time (t) diagrams recorded during asymmetric etching of PET foils containing a single Au ion track. Etching solution: 9 M NaOH. Stopping solution: 1 M KCl/1 M HCOOH. A) The current was recorded continuously at a bias voltage of 1 V. The electrode in the etching compartment of the cell is positive. The voltage of such polarity is denoted as "stopping voltage." B) The stopping voltage was periodically switched on and off, in each case for 5 min.

applied voltages as high as 10–30 V, the pore shape is affected dramatically.[25] On the contrary, in the absence of an applied voltage, there is no external influence but also no online information available about the pore evolution. The pore remains a "black box" and the information about its geometry and dimensions can only be obtained off-line, i.e., after the etching is completed and the sample is subjected, e.g., to scanning electron microscopy (SEM) examination. The SEM studies of membranes with asymmetric pores are described in the following Section 2.2.

Although an enlargement of the pore without the bias voltage does occur, the process seems to be very slow, and the diffusive mixing of the stopping solution and the etchant in the pore can hardly account for this effect. The concentration of alkali in the etchant is very high (9 mol L^{-1}), and its dilution down to a concentration of close to zero in the tip region exclusively due to alkali diffusion seems unlikely. To slightly open the "black box" and gain additional knowledge of the mechanisms of the initial stage of asymmetric etching, we performed osmotic flow measurements that can be applied to multipore membranes (for single-pore membranes the osmotic flow

effect would be too small). The results of this nondestructive monitoring of the etching process are presented and analyzed in Sections 2.3 and 2.4.

2.2. FESEM Observation of Asymmetric Pores

Multitrack samples were subjected to asymmetric etching using different stopping solutions, as described in the Experimental Section. Etching times were chosen to be longer than the typical breakthrough time found from conductometric experiments with single tracks. No bias voltage was applied to the multitrack samples, i.e., the etching was performed in the absence of an external electric field. To produce brittle samples and fracture them for cross-sectional FESEM imaging, the PET samples were exposed to extensive ultraviolet (UV) light as described in the Experimental Section. **Figure 2** shows representative longitudinal pore profiles obtained by this procedure. Image A presents pores that just reached the upper foil surface. The pore channels are approximately conical in shape with a double cone angle (2α) of 3.0°–4.5°. The pores have a geometry typical of etched ion tracks, which is described with a microscopic model that includes two basic parameters, namely, the bulk etching rate (V_B) and the track etching rate (V_T).[11] The track to the bulk etch rate, V_T/V_B, determines the cone angle of the etched channel: $\alpha = \arcsin(V_B/V_T)$. For tracks of Au ions in polyethylene terephthalate foils and the given UV-sensitization and etching conditions (9 M NaOH, room temperature), typical values of V_T and V_B are 75 and 2.0 nm min^{-1}, respectively. Image B in Figure 2 shows pores after a longer dwell time under asymmetric etching conditions. The conical sections of the pores widen uniformly so that the cone angle remains nearly constant. By contrast, the tips of the pores become rounder with increasing etching time. Note that the upper surface of the foil shown in Figure 2B seems to be free of any visible pores. The pore openings on the surface remain too small to be detected at the magnification used.

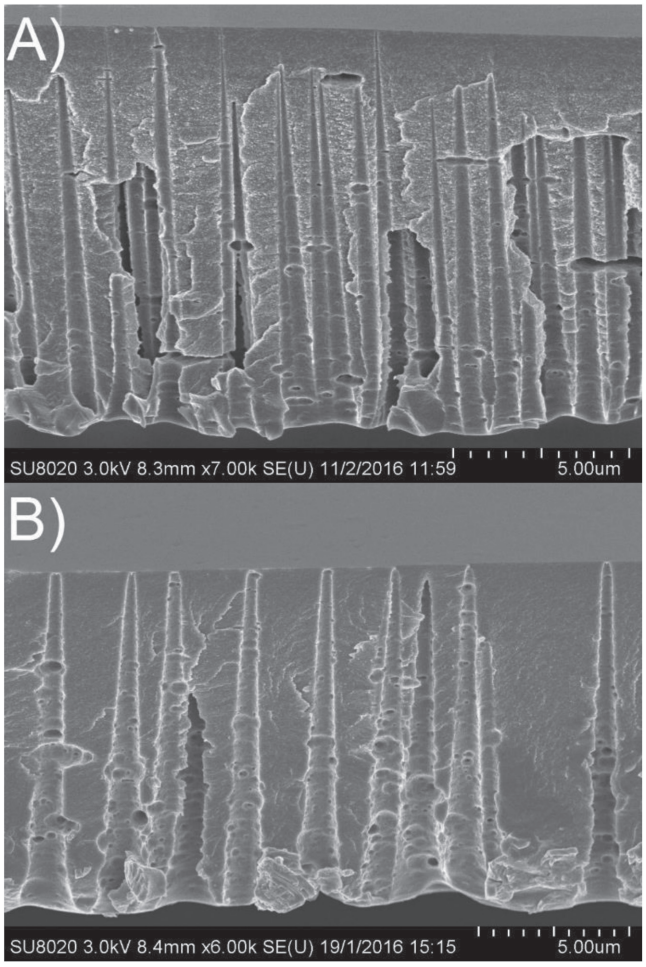

Figure 2. FESEM images of pores produced by asymmetric etching under different conditions. The PET foil was irradiated with Au ions. Etching solution: 9 M NaOH. Stopping solution: A) 1 M KCl/1 M HCOOH and B) 1 M HCOOH. The etching times were A) 120 min and B) 250 min. No stopping voltage was applied during the etching.

The FESEM images in **Figure 3** present the evolution of the pore tips in more detail. At the moment of breakthrough, the pore tip is a very narrow channel of few nanometers in radius (Figure 3A). While the wide part of the pore is conical, the narrow part is trumpet-shaped so that the very tip is nearly a cylinder of ≈1 µm in length.[32,33] As the etching proceeds, the tip geometry undergoes a considerable alteration. The length of the narrow tip region becomes shorter, decreasing down to nanometers. For longer etching times, the end of the pore acquires an approximately semispherical shape with a nanometer-sized hole that connects the inner volume of the pore and the upper surface of the foil. In Figure 3E, this hole is blocked by a nanosized precipitate identified as magnesium hydroxide crystals formed due to the presence of magnesium traces in the reagent used (KCl).[36]

Therefore, the growth of an ion track pore under asymmetric etching conditions can be illustrated as sketched in **Figure 4**. The inner pore profile depicted by a dashed line corresponds to the moment of breakthrough, t_b. At this stage, the pore has the shape of a cone with an elongated trumpet-like tip.[36] The outer pore profile depends on $t = t_b + t_{aba}$, where t_{aba} is the time of asymmetric etching after the breakthrough. The etching proceeds at the rate V_B on the right foil surface exposed to the etching solution and inside the pore, excluding the very tip region. The tip radius grows at a rate substantially slower than V_B. Such an evolution of the pore shape indicates that the etchant concentration in the pore is nearly constant along its length and dramatically drops in the tip region. The alkali gradient is essentially nonlinear suggesting that diffusion is not the only process of ion transport in the pore. Nonlinear gradients in narrow channels are typical for situations where the ion transport is governed by both diffusion and convection.[8] To reveal the role of convective transport in the asymmetric pores, we performed a series of dedicated experiments.

2.3. Osmotic Flow during Asymmetric Etching

Because the electrolyte concentrations on the two sides of the asymmetrically etched foil are considerably different, a gradient of the chemical potential of water across the foil exists, and the osmotic pressures of the etching and stopping

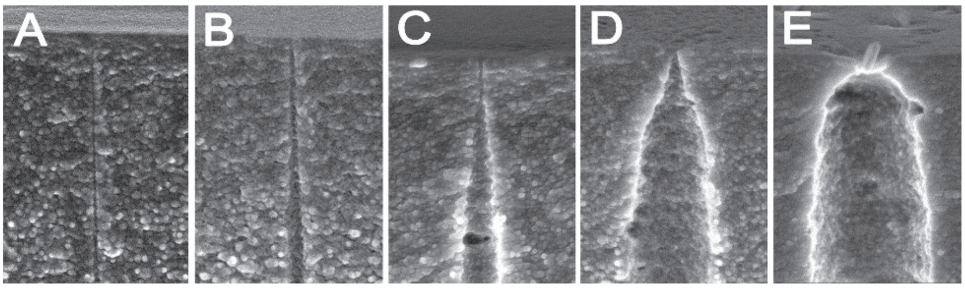

Figure 3. A–E) Tips of asymmetric pores at different stages of etching. The etching time increases from left to right. The PET foil was irradiated with Au ions. No stopping voltage was applied during etching. A) A pore tip that closely corresponds to the breakthrough moment. In the case of pore (E), the etching continued for ≈150 min after breakthrough. A nanosized crystalline precipitation is seen in the lumen of pore (E). The horizontal size of each image is 1000 nm.

solutions are important parameters that should be considered. According to the van't Hoff equation, the osmotic pressure difference ($\Delta\Pi$) is

$$\Delta\Pi = \Delta c\, RT \tag{1}$$

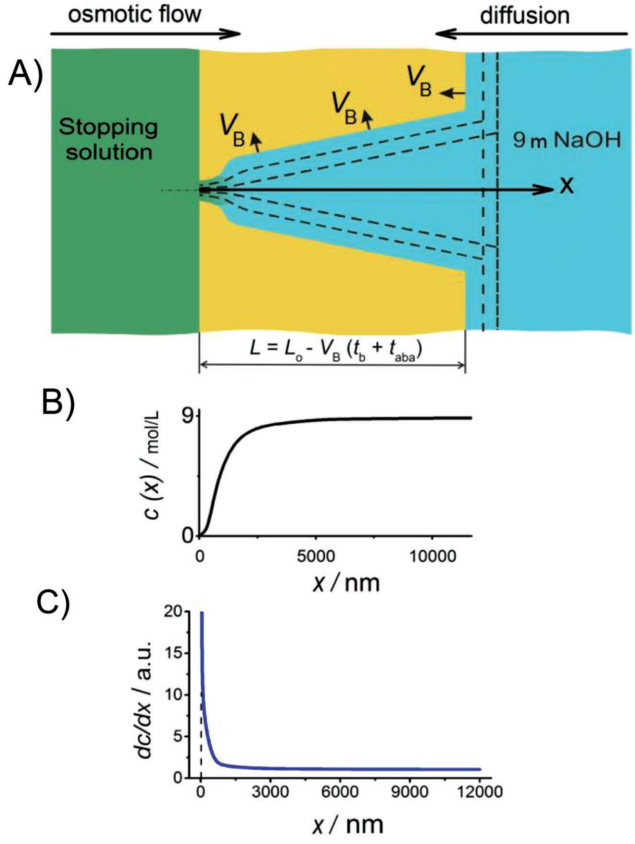

Figure 4. A) Scheme of asymmetrically etched pore in the initial stage after breakthrough. The conical part of the pore widens at a constant rate, V_B. The radius of the tip remains almost unchanged, which results in a pronounced transformation of the profile of the pore tip. B) Qualitative representation of the profile of the alkali concentration $c(x)$ anticipated from the pore shape. C) The alkali concentration gradient (dc/dx) calculated using formula (3). The input parameters are: $Q = 10^{-12}$ cm^3 s^{-1}, $b = 0.0275$, $r = 3$ nm, and $D = 10^{-5}$ cm^2 s^{-1}. The dc/dx function is normalized to its value at $x = L$.

where Δc is the difference in solute concentration, R is the universal gas constant, and T is the temperature. In the experiments on asymmetric etching, the difference in solute concentration between the two cell compartments is large and the differential osmotic pressure could reach appreciably high values. To measure the osmotic flux, the cell compartment filled with alkaline solution was equipped with a capillary (see Figures S1 and S2, Supporting Information).

Figure 5 shows the results of a series of experiments that demonstrate a considerable osmotic flow through asymmetrically etched ion tracks. The solution build-up (H) in the capillary as a function of etching time is presented for PET foils irradiated with three different ions. Additionally, two different stopping solutions—a neutral and an acidic one—were employed. The array of 10^8 Au ion tracks shows a well-pronounced osmotic flow that starts at 90–100 min and 140–200 min for the neutral and acidic stopping solutions, respectively (see Figure 5A). The etching rate along the Au ion tracks is calculated by dividing the initial foil thickness (L_o = 12 µm) by the time when the start of the flow through the pores is indicated by the steep increase in H. For the neutral stopping solution (1 M KCl), the track etching rate is ≈0.12 µm min^{-1}, while for the acidic stopping solution this quantity is approximately 1.5-fold to 2-fold smaller. Tracks of lighter ions (Xe and Kr), which possess lower energy losses in the polymer (see **Table 1**) and produce weaker damage along their trajectories, are etched through at slower rates. Interestingly enough, the resulting pores show a similar osmotic flow. The fact that the composition of a stopping solution affects the track etching rate unambiguously indicates that the unetched track is partially permeable to electrolytes and that soaking the track in an acidic agent (formic acid in our case) slows down the alkaline etching. Indeed, the track consists of heavily damaged polymer, contains a high concentration of carboxylic groups and increased free volume due to amorphization and outgassing of volatile degradation fragments. At low pH, the carboxylic groups are protonated, which results in a decrease in the ionic permeability of the tracks.[37,38] It is remarkable that the effect of the acidic stopping solution on the breakthrough time decreases with decreasing energy loss of the ion that produced the track. The relative difference among the times of the through etching of Kr ion tracks caused by different pH values of the stopping solution is ≈30% on average (see Figure 5C). We assume this is ascribed to the fact that carboxylic groups play the role of a pH-sensitive promoter of electrolyte diffusion

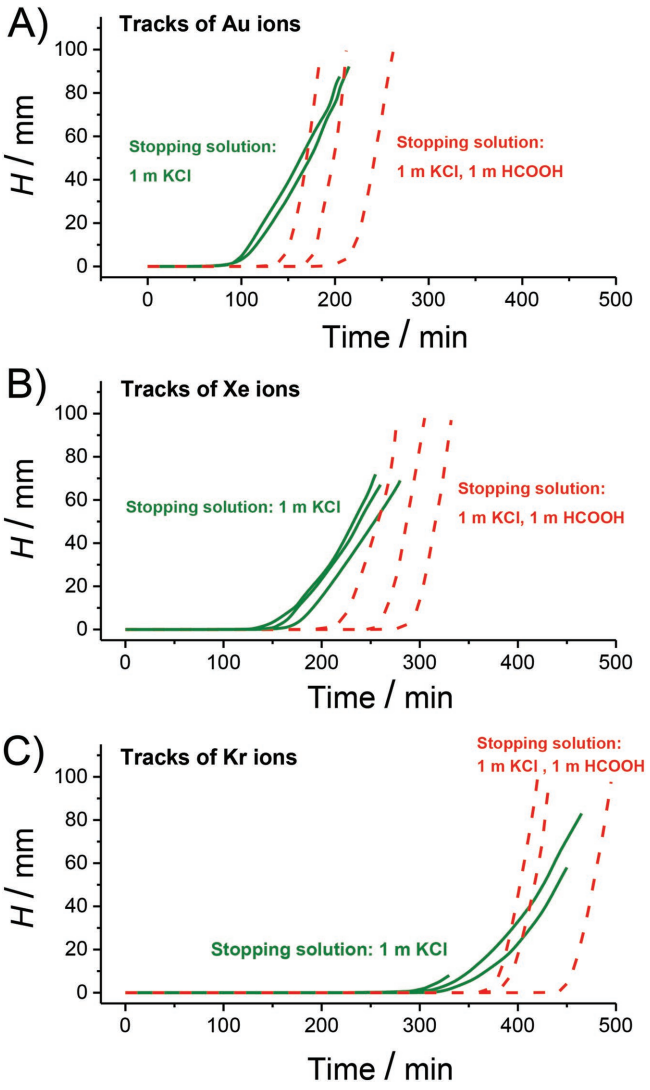

Figure 5. Build-up of solution level (H) in the alkaline compartment of the cell as a function of asymmetric etching time. Etching solution: 9 M NaOH. Stopping solution: 1 M KCl (solid green lines) and 1 M KCl/1 M HCOOH (dashed red lines). The PET foils contain ≈10^8 tracks produced with A) Au, B) Xe, and C) Kr ions. The results of several independent experiments for each set of parameters (ion and stopping solution) are shown.

through damage trails produced by energetic ions.[38] As a consequence of lower dissipated energy the latent tracks of lighter ions contain fewer carboxylic groups, and the etchant penetration into the tracks is substantially slower and less influenced by pH.

The osmotic flux (Q) through one pore can be deduced from the slopes of the H versus time curves, the cross-sectional area of the measuring capillary, and the number of pores. For the acidic stopping solution, the flux takes a value of $\approx 1 \times 10^{-12}$ cm^3 s^{-1} soon after breakthrough and then reaches an approximately constant level of $\approx 7 \times 10^{-12}$ cm^3 s^{-1} (data for Au ion tracks in Figure 5A). Immediately after breakthrough, the tip radius (r) is typically 3–5 nm, and after an additional 90 min etching, it does not exceed 10 nm.[36] Under the assumption that the osmotic flux is radially uniform, the linear velocity of the volume flow can be calculated by dividing the Q value by the cross-sectional area S_p of the pore. In the pore lumen, the velocity reaches a value of ≈1 cm s^{-1}. Along the conical pore with a cone angle 2α, the velocity decreases proportionally to the reciprocal of the squared pore radius.

To semi-quantitatively describe the alkali distribution $c(x)$ within the asymmetric pore, a diffusion–convection model is suggested. Since the etching process at room temperature is slow, we can use the stationary diffusion–convection equation valid for a certain instant of time[39]

$$-\frac{Q}{S_p(x)}\frac{dc}{dx} = D\frac{d^2c}{dx^2} \quad (2)$$

where $S_p(x)$ is the cross-sectional area of the pore; x is the distance along the pore axis, and points $x = 0$ and $x = L$ are located at the opposite sides of the foil; and D is the diffusivity of sodium hydroxide. For simplicity, we assume that the concentration is uniform in each cross-section of the pore and that the diffusion coefficient does not depend on concentration. Since ionic strength of both the etchant and the stopping solution is very high, we neglect any effects of surface charge on the distribution of ions in the pore channels. We also neglect other solutes (KCl, HCOOH) which are present in relatively small concentrations. For a conical pore, the radius changes along the x-axis as $r + bx$, where b depends on the cone angle. Accordingly, we obtain for the pore cross-sectional area, $S_p(x) = \pi (r + bx)^2$. Inserting this expression into Equation (2) yields a differential equation, the general solution of which is tedious, but the concentration gradient can be easily found

$$\frac{dc}{dx} = A\exp\left(Q/\pi D\, b^2 (x + r/b)\right) \quad (3)$$

where A is a constant. Taking a typical conical pore with $r = 3$ nm and $b = 0.0275$ (which corresponds to a cone angle (2α) of 3.2°), we calculated the alkali gradient that forms in the newborn pores, i.e., just after breakthrough. For the diffusion coefficient D, in a concentrated sodium hydroxide solution, a value of 10^{-5} cm^2 s^{-1} was taken from the literature.[40] The result is shown in Figure 4C. The modeling clearly shows that the alkali concentration gradient is very high in the tip region ($x < 1000$ nm), while in the wide part of the pore, the alkali concentration changes only slightly along the pore axis. This is a direct consequence of the osmotically driven water flow into the pore. Because of the osmotic flow, the short pore tip is depleted of etchant molecules and does not widen for a rather long time after breakthrough. It should be stressed that the concentration profile in the tip region is very sensitive to variations in the cone angle, 2α.[36] For this reason the shapes of the pore tips in Figure 3 are only representative for a given set of ion and etching conditions providing a track-to-bulk etch rate ratio of ≈40. An increase in the cone angle leads to a shortening of the rounded pore tip and vice versa.

As seen from the slopes of the H versus time curves presented in Figure 5, not only the track etching rate but also the value of osmotic flux depends on the acidity of the stopping solution. For tracks of all three ions (Au, Xe, and Kr), the osmotic flux is higher when the foil is in contact with the

Table 1. Energy and energy loss dE/dx of ions used to produce nanopores in PET foils.

Ion	Kinetic energy [MeV]	dE/dx[46] [keV nm^{-1}]
Au	1100	15–17
Xe	160	8–11
Kr	100	3–6

solution containing formic acid. Previously, it was hypothesized that this phenomenon originates from different shapes of pores fabricated using different stopping solutions.[36] To check this hypothesis, we modified the experimental procedure in the following way. Using a neutral stopping solution (1 M KCl), an array of tracks was etched asymmetrically until a stable osmotic flux developed. The neutral stopping solution was quickly replaced with an acidic one (1 M KCl/1 M HCOOH), and the measurement of osmotic flow was continued. A typical result is presented in **Figure 6**. Just after the replacement of the stopping solution, the slope of the etchant level build-up markedly increased. Therefore, the higher osmotic flux from the acidic stopping solution is not caused by a different pore configuration. The pore geometry cannot change considerably within the time interval of 1–2 min. Rather, the reason for the observed phenomenon is very simple and constitutes a common mechanism affecting the membrane permeability in the process of forward osmosis. The lower-than-expected water flux is often attributed to concentration polarization (CP) phenomena.[41] When the feed solution flows on the active layer of a semipermeable membrane, solute builds up at the membrane surface. This is called concentrative external CP. Simultaneously, the draw solution in contact with the other side of the membrane is being diluted at the permeate–membrane interface by the permeating water. This is called dilutive external CP. Both types of CP reduce the effective osmotic driving force. Track-etched membranes are not semipermeable; in the literature, such membranes are categorized as membranes with leaky pores. Both water and solute diffuse through the pores, driven by differences in relevant concentrations across the membrane. The water flux dominates among osmotic fluxes of other solution

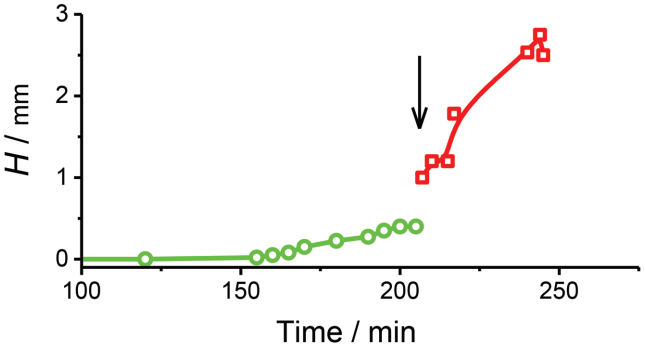

Figure 6. The derivative of the etchant solution build-up, dH/dt, as a function of time (green circles: stopping solution 1 M KCl, red squares: stopping solution 1 M KCl/1 M HCOOH). The vertical arrow indicates the moment when 1 M KCl was replaced with 1 M KCl/1 M HCOOH. The sample was a PET foil containing ≈10^8 tracks of Xe ions.

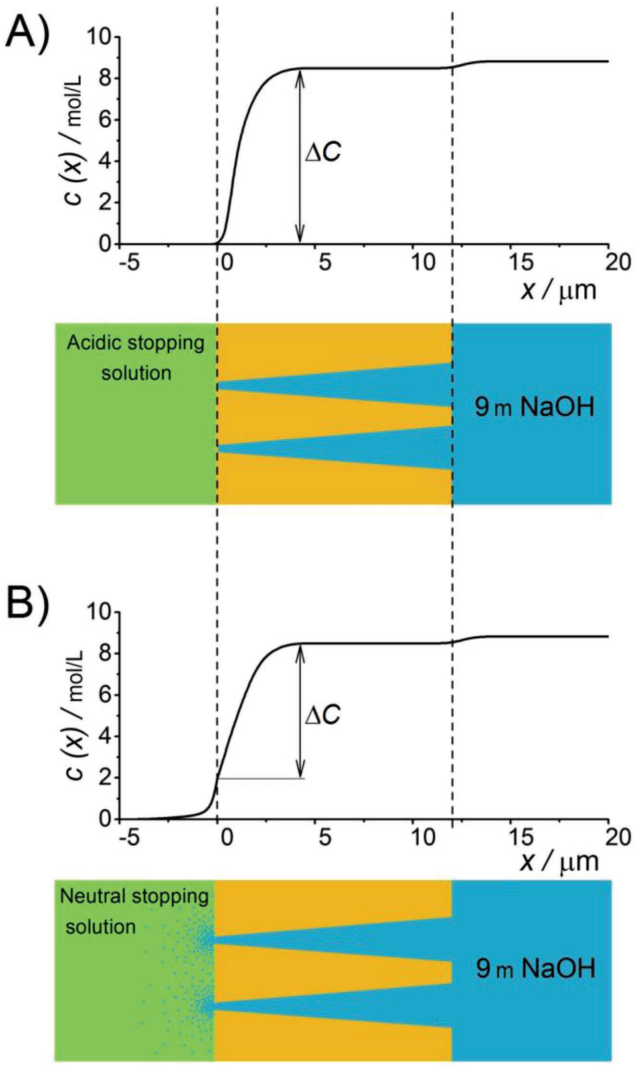

Figure 7. Alkali concentration profiles $c(x)$ across an asymmetric membrane in contact with A) acidic and B) neutral stopping solutions. The concentration difference (Δc) determines the driving force for the osmotic flow.

components, however, the diffusion of alkali in the opposite direction should also be considered. When hydroxide ions diffuse into an acidic stopping solution, a chemical reaction with formic acid occurs

$$OH^- + HCOOH \rightarrow H_2O + HCOO^- \quad (4)$$

Two particles of solutes are converted into one solute particle and one water molecule. As a result, the total concentration of solutes decreases, and the concentration of alkali is close to zero at the membrane surface, as shown in **Figure 7**A. By contrast, diffusion of hydroxide ions into the neutral stopping solution leads to an increase in the alkali concentration in the layer adjacent to the membrane surface (see Figure 7B). In this case, the concentration drop (Δc) across the pore decreases, which leads to a lower gradient of the water chemical potential and, accordingly, to a lower osmotic flux, compared with the situation with the acidic stopping solution.

In this section we offered a model based on a number of simplifications—including ideal cone geometry, steady state, constant diffusion coefficient, uniform concentration in each cross-section, and negligible surface charge. However, a rigorous approach should be free of the listed assumptions and consider, in particular, the influence of electrical surface charge. Chemically etched PET surface is negatively charged at medium and high pH.[12] Therefore, the effects of electrical double layer (EDL) should be taken into account. At present we do not know the electrolyte concentration in the very tip region and cannot estimate the thickness of EDL. It is known that charged nanopores whose radius is much larger than the Debye length can exhibit ionic selectivity.[42] Therefore, though the alkali concentration in the etching solution is very high, the influence of surface charge on the mobile ion concentration gradient and the chemical potential gradient of water in the narrowest part of the pore cannot be ruled out. Clarifying this question can be a good challenge for future studies of osmotic phenomena in asymmetrical track-etched nanopores.

2.4. Osmotic Flow through Pre-Etched Cylindrical Nanopores

As we showed in the previous section, the interplay between diffusion and convection fluxes in conical nanopores leads to the formation of a steep gradient of etchant in the narrow part of the pore, which strongly affects further evolution of the channel. In this section, we explore membranes with cylindrical pore geometry that are easily obtained using the track etching technique. Ion-irradiated PET foils were pre-etched under high track-to-bulk etch rate ratio conditions yielding pores of cylindrical shape (see the Experimental Section and Figure S1B of the Supporting Information). Subsequent measurements of osmotic flow through pre-etched porous membranes were performed by the same procedure, as described above.

Figure 8A shows the development of osmotic flux through the membrane with cylindrical pores (diameter ≈30 nm) during continued asymmetric etching. In the beginning of the process, the volume flow rate is $\approx 8 \times 10^{-4}$ cm^3 min^{-1}, which corresponds to a linear water flow velocity in the pore of $v \approx 1.8 \times 10^{-2}$ cm s^{-1}. A tenfold increase in the volume flow is observed after 55 min etching. Figure 8B,C presents FESEM images of the membrane before and after continued asymmetric etching. The pre-etched membrane shows narrow cylindrical channels (Figure 8B). After continued asymmetric etching, the channels consist of a long cylindrical part, ≈9 µm in length and 200 nm in diameter, and a conical tip with the length of ≈3 µm (Figure 8C). The channel profile obviously reflects the alkali distribution along the pore axis. The diffusion–convection equation for a cylindrical geometry is

$$-\frac{v}{D}\frac{\mathrm{d}c}{\mathrm{d}x} = \frac{\mathrm{d}^2 c}{\mathrm{d}x^2} \tag{5}$$

where v is the linear flow velocity of the solution. Assuming that there is no concentration polarization on both sides of the membrane, we take $c(x = 0) = 0$ and $c(x = L) = c_0$. The solution to Equation (5) is

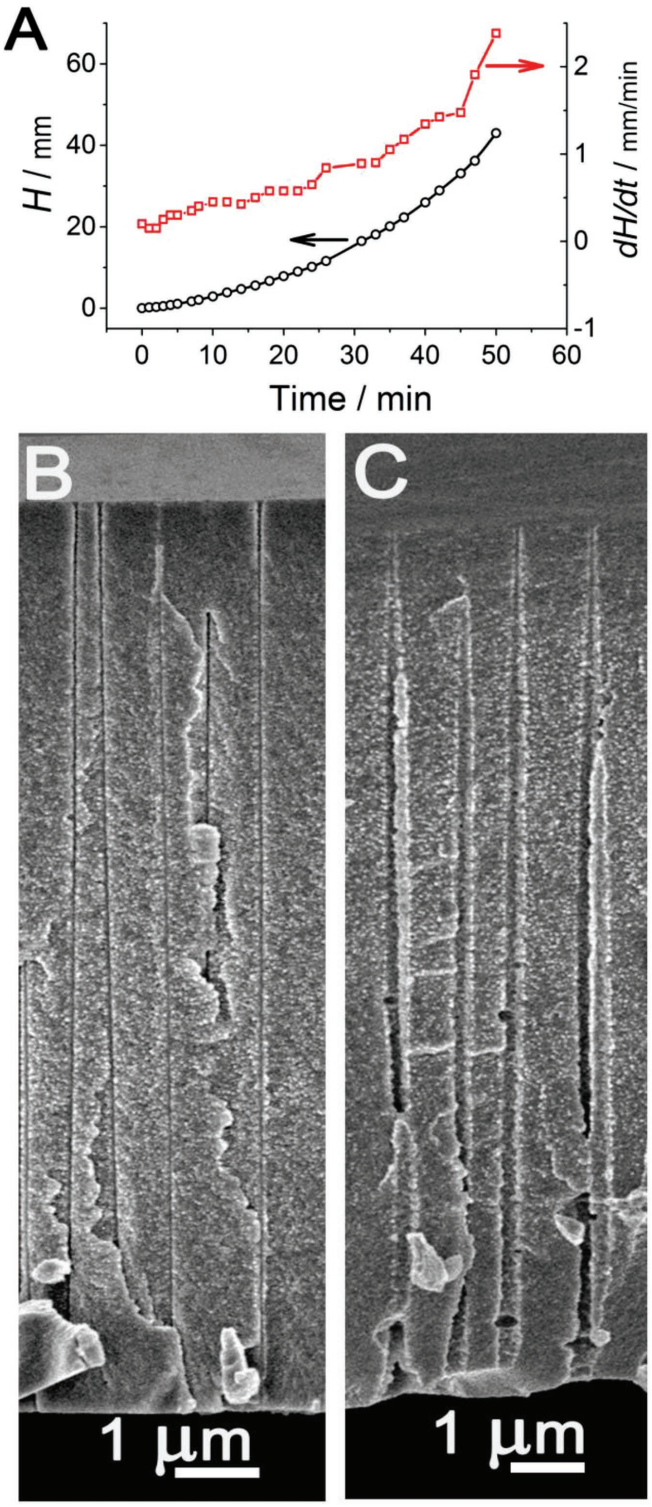

Figure 8. A) Build-up of the alkali solution level (H) and its derivative (dH/dt) as functions of the asymmetric etching time of a membrane with pre-etched cylindrical pores ≈30 nm in diameter. Pore density: 1.0×10^8 cm^{-2}. Sample working area: 1 cm^2. Etching solution: 9 M NaOH. Stopping solution: 1 M KCl/1 M HCOOH. SEM images of B) cylindrical pores before asymmetric etching and C) after 55 min asymmetric etching.

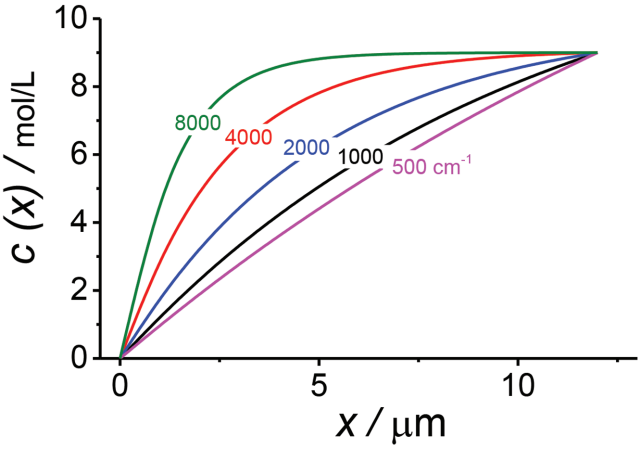

Figure 9. Alkali concentration profile $c(x)$ in a cylindrical pore with a length of 12 µm, calculated for different values of parameter v/D [cm^{-1}] as indicated in the plot.

$$c(x) = \frac{c_o\left(1 - e^{-v\frac{x}{D}}\right)}{1 - e^{-vL/D}} \tag{6}$$

The functions $c(x)$ are shown in **Figure 9** for c_o = 9 mol L^{-1} and different values of the parameter v/D. The larger the v to D ratio, the stronger the deviation of the concentration profile from linearity. The pore shape with a long cylindrical part and a relatively short tapered region can be obtained when v/D is as large as ≥8000. In our experiment, we found $v \approx 1.8 \times 10^{-2}$ cm s^{-1}, and a D value of $\approx 1 \times 10^{-5}$ cm^2 s^{-1} can be taken for a concentrated sodium hydroxide solution. With such values for the input parameters, we cannot expect the formation of a pore with a short, tapered end. According to the calculation, the pore profile at v/D = 1800 should rather be close to conical. To explain the pore shape observed experimentally, it can be hypothesized that the diffusion coefficient in the narrow channel is lower than 1×10^{-5} cm^2 s^{-1}. Several reasons for that can be suggested. First, diffusion in a restricted volume can be hindered due to interactions with the pore walls. Second, the etching products (sodium terephthalate) have a very low solubility in highly alkaline solutions and can affect the mobility of ionic species in the narrow channel. However, it should be realized that a sufficient etching time can lead to a pore shape with a tapered end, even if the v/D values are relatively small in the beginning. Indeed, in the first phase of the process, the cylindrical pore is transformed into a slightly conical one. Equation (5) is no longer valid for this geometry, and the second phase, described by Equations (2) and (3), comes into play. Simultaneously, the osmotic flux increases, and the parameter v also takes a higher value. These alterations result in an increasingly steep concentration gradient in the narrow region of the pore and eventually lead to a sharply tapered tip. This hypothesis is supported by the observation of the pore profiles obtained with neutral stopping solutions, when the osmotic flow was very weak in the beginning of the asymmetric etching (see Figure S3 in the Supporting Information) and increased greatly after 30–50 min of etching. The pores fabricated in this way have well-pronounced tapered tips. Note that pores of this geometry have been observed previously.[25] The asymmetric etching of ion tracks in a polycarbonate foil with no applied potential yielded a pore that was "nearly cylindrical through most of its length with a conical segment of about 3 µm at one end."[25] This pore shape can be explained in the following way. The track-to-bulk etch ratio in polycarbonate is very high and, therefore, a cylindrical pore formed in the first stage of etching. Later, the osmotic pressure gradient triggers the mechanism described above, which eventually leads to the formation of a conical tip. Thus, this mechanism holds for nanopores in polymer foils other than PET.

The experiments with pre-etched ion track nanopores show that pronounced osmotic phenomena can be observed with a small molecule ionic solute and channels as wide as 30 and even 60 nm (see the Supporting Information). The question arises as to why this finding has not been reported before during the more than 50-year history of track-etched membranes. One of the reasons lies in the fact that experiments on osmosis are normally performed with nonaggressive solutes, i.e., with substances that do not damage the membrane. The overwhelming majority of studies have dealt with neutral salts and have focused on applications where the lifetime of membranes should be as long as possible. By contrast, we employed a solute that could attack the membrane material. This property of our draw solution made it possible to extract information on the solute concentration gradients within pores at the sub-micrometer scale. The pores served as a substrate for imprinting the etchant concentration field, which, in turn, was used to understand the balance between the diffusion and convection transport of alkali ions. Another important feature of sodium hydroxide as solute is its ability to strongly reduce the activity of water. Most of the other electrolytes have a weaker effect on the water activity. It should be mentioned that Equation (1) is valid only for ideal solutions, while for strong alkaline etchants an approach based on chemical potential theory is more appropriate. In terms of chemical potential, the driving force for the solvent osmotic flow is determined by the solvent molar concentration (c_s (mol/mol)) gradient and the solvent activity coefficient (γ_s)[43]

$$\Delta\mu_s = RT\,\Delta\mathrm{In}\left(\gamma_s c_s\right) \tag{7}$$

where μ_s is the chemical potential of the solvent (water in our experiments). In 9 M NaOH, the activity of water drops down to ≈0.52.[44] This specific feature of strong alkaline solutions makes the observation of osmotic phenomena easier than with neutral electrolytes. However, the fabricated asymmetric membranes in this work show osmotic flow also when the draw solution was prepared from sodium chloride (see Figure S5, Supporting Information).

3. Conclusions

Under asymmetric etching of ion tracks, osmotic flow is built up with the etchant playing the role of the draw solution. Measuring the osmotic flux makes it possible to monitor the formation and evolution of through channels in the early pore formation stage. On-line monitoring of the osmotic flux

through multitrack samples provides information not available by conductivity measurements due to the very low electrical resistance of large arrays of parallel pores filled with electrolyte. Osmotic flow is responsible for a dramatic dilution of the etchant in the pore tip when etching continues after breakthrough. This effect keeps the pore radius at a level of several nanometers for a while constant. Our results on the osmotic flow in combination with SEM data indicate that the geometry of the asymmetric pores is determined by the interplay between diffusion and the osmotically driven convective transport of the etchant. The velocity of the convective transport as estimated from the measured osmotic flux can be used to calculate, at least semi-quantitatively, the gradient of the etchant concentration. The latter determines the pore shape. Understanding this mechanism and adjusting the osmotic pressures of solutions employed for asymmetric etching provides control over the pore shape complementing existing methods such as bias voltage, external pressure, and organic solvents in the etching solution.

4. Experimental Section

Ion Irradiation: Polyethylene terephthalate biaxially oriented foils (12 µm thick Hostaphan RNK, Mitsubishi Polyester Films) were irradiated with single and multiple (fluences of 10^7–10^8 cm^{-2}) Au ions at the UNILAC facility of GSI (Darmstadt). Stacks consisting of 4–5 samples were exposed at normal incidence. The initial kinetic energy of the projectiles was 1.1 GeV. For gold ions of such high kinetic energy, the energy loss when passing through the foil stack varies by only ≈10% (see Table 1). Therefore, the properties of the tracks in the different PET layers can thus be regarded as nearly constant.[45] Similar irradiations were performed with 160 MeV Xe and 100 MeV Kr ions at the IC-100 cyclotron (FLNR JINR, Dubna). The energy and the energy loss of the ions are summarized in Table 1.

Track Sensitization and Etching, Osmotic Flow, and Electrical Measurement Conditions: To sensitize the ion tracks and increase the track-to-bulk etch ratio, all ion-irradiated samples were exposed from one side for 60 min to soft ultraviolet radiation (wavelength > 315 nm, with a pristine 12 µm thick PET foil used as filter). The intensity of the UV radiation at the sample surface was ≈2.5 W m^{-2} (measured by a UV radiometer TKA-PKM, model 12, Russia).

The etching of single-track and multitrack samples was performed in a two-compartment electrolytic cell.[13] One compartment was filled with 9 M NaOH, and the other compartment contained a stopping solution. Different stopping solutions were used including aqueous 1 M KCl and 1 M HCOOH solution as well as a mixture of 2 M KCl and 2 M HCOOH (50:50, v/v), referred to as 1 M KCl/1 M HCOOH throughout the paper. Conductometric monitoring of the etching process for single-track samples was performed in DC mode using a PC-controlled Keithley 6482 picoammeter (Keithley Instruments, Cleveland, OH). A bias voltage of 1 V was applied to the gold electrodes (1 cm^2 surface area), always with the positive sign on the alkali side.

To observe and measure the osmotic flow through newborn pores in PET foils during asymmetric etching, the cell was equipped with a fluoropolymer capillary, with a 2 mm inner diameter.[36] The capillary was inserted into the compartment with the alkaline solution (see Figures S1 and S2, Supporting Information). The track density in the foils was in the range of 10^7–10^8 cm^{-2}. The actual track densities were determined using SEM with a statistical error not exceeding 5%. The total area of the sample was 2.8 cm^2; however, only a central circle of 1 cm^2 was sensitized with UV light, as shown in Figure S1 (Supporting Information). The tracks in the sensitized area are etched more rapidly than the nonsensitized tracks outside the circle. This avoided pore formation at the edges of the sample and thus avoided disturbances caused by air bubbles, mechanical strain, and other irregularities. The elimination of air bubbles on the porous area of the foil in the compartment with the stopping solution was especially important to provide conditions for the observation of osmotic phenomena. The inner volume of each compartment of the cell was 3 cm^3. All etching experiments were performed at an ambient temperature of 22–23 °C.

Small-pore track-etched membranes with cylindrical pores were fabricated using PET foils irradiated with 10^8 Xe ions cm^{-2}. After sensitization with UV light through the 1 cm^2 diaphragm, the samples were etched in 2 M NaOH at 60 °C for 195 s (Figure S1B, Supporting Information). The airflow rate through the pores at a pressure difference of 0.15 bar was 1.2 mL min^{-1} yielding an effective pore diameter of 32 nm. Membranes with a pore density of 10^9 cm^{-2} and effective pore diameter of 62 nm were fabricated in a similar way using a slightly longer etching time.

Ultrapure water, 18.2 MOhm cm from Arium (Vladisart) and reagent grade chemicals from Sigma Aldrich were used for solutions preparation.

Electron Microscopy: After the etching process was stopped, the samples were rinsed with deionized water and air-dried. Electron microscopy investigations were performed on multitrack samples using an FESEM instrument (Hitachi SU8020, Japan). The surface of the samples was sputter-coated with a 10 nm thick chromium layer. To image the smallest pores (20–50 nm), uncoated samples were examined using the deceleration voltage mode of the microscope.

The geometry of the pores was determined by imaging cross-section of fractured samples. A photooxidation technique based on UV exposure was applied to render the initially flexible polymer films brittle.[47] The UV exposed specimens easily broke when touched with tweezers.

Supporting Information

Supporting Information is available from the Wiley Online Library or from the author.

Acknowledgements

The authors are grateful to A. Olejniczak for his help with programming the measuring instruments. The authors thank O. A. Polezhaeva for assistance in the experiments.

Conflict of Interest

The authors declare no conflict of interest.

Keywords

convection, diffusion, etching, ion track nanopores, osmotic flow

Received: September 25, 2017
Revised: February 5, 2018
Published online: March 24, 2018

[1] A. Mauro, *Science* **1957**, *126*, 252.
[2] E. A. Marshall, *J. Theor. Biol.* **1977**, *66*, 107.
[3] A. Hill, *Q. Rev. Biophys.* **1979**, *12*, 67.
[4] A. Hill, *Proc. R. Soc. London, Ser. B* **1982**, *215*, 155.
[5] A. Hill, *Proc. R. Soc. London, Ser. B* **1989**, *237*, 369.
[6] A. Hill, *J. Membr. Biol.* **1994**, *137*, 197.
[7] J. S. Schultz, R. Valentine, C. Y. Choi, *J. Gen. Physiol.* **1979**, *75*, 49.
[8] S. R. Thomas, D. C. Mikulecky, *Microvasc. Res.* **1978**, *15*, 207.

[9] L. Zeman, M. Wales, *Sep. Sci. Technol.* **1981**, *16*, 275.
[10] W. D. Comper, R. P. W. Williams, *Biophys. Chem.* **1990**, *36*, 215.
[11] R. L. Fleischer, P. B. Price, R. M. Walker, *Nuclear Tracks in Solids*, University of California Press, Berkeley, CA **1975**.
[12] P. Apel, *Radiat. Meas.* **2001**, *34*, 559.
[13] P. Y. Apel, Yu. E. Korchev, Z. Siwy, R. Spohr, M. Yoshida, *Nucl. Instrum. Methods Phys. Res., Sect. B* **2001**, *184*, 337.
[14] Z. Siwy, P. Apel, D. Dobrev, R. Neumann, R. Spohr, C. Trautmann, K. Voss, *Nucl. Instrum. Methods Phys. Res., Sect. B* **2003**, *208*, 143.
[15] Z. S. Siwy, *Adv. Funct. Mater.* **2006**, *16*, 735.
[16] R. E. Gyurcsanyi, *Trends Anal. Chem.* **2008**, *27*, 627.
[17] I. Vlassiouk, T. R. Kozel, Z. S. Siwy, *J. Am. Chem. Soc.* **2009**, *131*, 8211.
[18] J. Cervera, P. Ramirez, S. Mafe, P. Stroeve, *Electrochim. Acta* **2011**, *56*, 4504.
[19] A. Kocer, L. Tauk, P. Dejardin, *Biosens. Bioelectron.* **2012**, *38*, 1.
[20] C. Duan, W. Wang, Q. Xie, *Biomicrofluidics* **2013**, *7*, 026501.
[21] C. Algieri, E. Drioli, L. Guzzo, L. Donato, *Sensors* **2014**, *14*, 13863.
[22] Z. D. Harms, D. G. Haywood, A. R. Kneller, S. C. Jacobson, *Analyst* **2015**, *140*, 4779.
[23] H. Zhang, Y. Tian, L. Jiang, *Nano Today* **2016**, *11*, 61.
[24] I. Enculescu, Z. Siwy, D. Dobrev, C. Trautmann, M. E. Toimil-Molares, R. Neumann, K. Hjort, L. Westerberg, R. Spohr, *Appl. Phys. A* **2003**, *77*, 751.
[25] C. C. Harrell, Z. S. Siwy, C. R. Martin, *Small* **2006**, *2*, 194.
[26] P. Scopece, L. A. Baker, P. Ugo, C. R. Martin, *Nanotechnology* **2006**, *17*, 3951.
[27] J. E. Wharton, P. Jin, L. T. Sexton, L. P. Horne, S. A. Sherrill, W. K. Mino, C. Martin, *Small* **2007**, *2*, 1424.
[28] M. Ali, V. Bayer, B. Schiedt, R. Neumann, W. Ensinger, *Nanotechnology* **2008**, *19*, 485711.
[29] W. Guo, J. M. Xue, W. M. Zhang, X. Q. Zou, Y. G. Wang, *Radiat. Meas.* **2008**, *43*, S623.
[30] W. Guo, J. Xue, L. Wang, Y. Wang, *Nucl. Instrum. Methods Phys. Res., Sect. B* **2008**, *266*, 3095.
[31] M. L. Kovarik, K. Zhou, S. C. Jacobson, *J. Phys. Chem. B* **2009**, *113*, 15960.
[32] P. Y. Apel, I. V. Blonskaya, O. L. Orelovitch, B. A. Sartowska, R. Spohr, *Nanotechnology* **2012**, *23*, 225503.
[33] P. Y. Apel, P. Ramirez, I. V. Blonskaya, O. L. Orelovitch, B. Sartowska, *Phys. Chem. Chem. Phys.* **2014**, *16*, 15214.
[34] L. J. Small, D. R. Wheeler, E. D. Spoerke, *RSC Adv.* **2014**, *4*, 5499.
[35] F. Roustaie, J. Bieker, R. Cicek, H. F. Schlaak, *Microelectron. Eng.* **2017**, *180*, 81.
[36] P. Y. Apel, V. V. Bashevoy, I. V. Blonskaya, N. I. Lizunov, O. L. Orelovitch, C. Trautmann, *Phys. Chem. Chem. Phys.* **2016**, *18*, 25421.
[37] V. V. Berezkin, A. N. Nechaev, S. V. Fomichev, B. V. Mchedlishvili, N. I. Zhitariuk, *Colloid J.* **1991**, *53*, 292.
[38] Q. Wen, D. Yan, M. Wang, Y. Ling, P. Wang, P. Kluth, D. Schauris, C. Trautmann, P. Apel, W. Guo, G. Xiao, J. Liu, J. Xue, Y. Wang, *Adv. Funct. Mater.* **2016**, *26*, 5796.
[39] C. Lee, C. Cottin-Bizonne, A.-L. Biance, P. Joseph, L. Bocquet, C. Ybert, *Phys. Rev. Lett.* **2014**, *112*, 244501.
[40] D'Ans und, E. Lax, *Taschenbuch für Chemiker und Physiker*, Springer-Verlag, Berlin Heidelberg **1943**, p. S.1115.
[41] T. Y. Cath, A. E. Childress, M. Elimelech, *J. Membr. Sci.* **2006**, *281*, 70.
[42] P. Ramirez, P. Y. Apel, J. Cervera, S. Mafe, *Nanotechnology* **2008**, *19*, 315707.
[43] J. G. Wijmans, R. W. Baker, *J. Membr. Sci.* **1995**, *107*, 1.
[44] G. Åkerlöf, G. Kegeles, *J. Am. Chem. Soc* **1940**, *62*, 620.
[45] P. Y. Apel, A. Schulz, R. Spohr, C. Trautmann, V. Vutsadakis, *Nucl. Instrum. Methods Phys. Res., Sect. B* **1998**, *146*, 468.
[46] J. F. Ziegler, J. P. Biersack, U. Littmark, *The Stopping and Range of Ions in Solids*, Pergamon, New York **1985**; Free SRIM software is available from the website, http://www.srim.org (accessed: February 2018).
[47] P. Y. Apel, I. V. Blonskaya, S. N. Dmitriev, O. L. Orelovitch, A. Presz, B. A. Sartowska, *Nanotechnology* **2007**, *18*, 305302.